A new probe of magnetic fields in the pre-reionization epoch: II. Detectability

Vera Gluscevic,[1] Tejaswi Venumadhav,[1] Abhilash Mishra,[2] Antonija Oklopcic,[2] Xiao Fang,[3] and Christopher Hirata[3]

[1] *Institute for Advanced Study, Einstein Drive, Princeton, NJ 08540, USA*
[2] *California Institute of Technology, Mail Code 350-17, Pasadena, CA 91125, USA*
[3] *Center for Cosmology and Astroparticle Physics, The Ohio State University, 191 West Woodruff Lane, Columbus, Ohio 43210, USA*

(Dated: March 17, 2016)

In the first paper of this series, we proposed a novel method to detect large-scale intergalactic magnetic fields during the Dark Ages, using future 21-cm tomography surveys. In this paper, we examine detectability of magnetic fields using this method. We first develop a minimum-variance estimator formalism that relies on identifying the characteristic anisotropic imprints in the 21-cm brightness-temperature 2-point correlation functions. We then perform Fisher forecast for this estimator and find that a radio array with a square kilometer tiled with dipole antennas can detect fields of strength on the order of 10^{-21} Gauss at redshift of 20, reaching almost 10 orders of magnitude below the current CMB constraints on primordial magnetic fields.

I. INTRODUCTION

Magnetic fields are ubiquitous in the universe on all observed scales [1–5]. However, the origins of the magnetic fields in Galaxies and on large scales are as of yet an unresolved question. Various forms of dynamo mechanisms are proposed to maintain and amplify magnetic fields [6], but they typically require "seed fields" to be present [1]. Such seed fields may be produced during structure formation through Biermann battery or similar mechanisms [7, 8], or may otherwise be relics from the early universe [1, 9, 10]. Observations of large-scale low-strength magnetic fields in the high-redshift intergalactic medium (IGM) can thus probe the origins of present-day magnetic fields, and potentially open up an entirely new window into the physics of the early universe.

Many observational probes have been previously proposed and used to search for evidence of large-scale magnetic fields locally and at high redshifts (e. g. [4, 11–19]). Amongst the most sensitive tracers of cosmological magnetic fields is the cumulative effect of Faraday rotation in the cosmic-microwave-background (CMB) polarization maps, which currently places an upper limit of $\sim 10^{-10}$ Gauss (in comoving units) using data from the Planck sattelite [20]. In Paper I of this series [21], we proposed a novel method to detect and measure extremely weak cosmological magnetic fields during the pre-reionization epoch (the cosmological Dark Ages). This method relies on data from upcoming and future 21-cm brightness-temperature tomography surveys [22, 23], many of which have pathfinder experiments currently running [24–29], with the next-stage experiments planned for the coming decade [27, 29].

In Paper I, we layed out the formalism necessary to account for the effect of magnetic fields on the statistics of the 21-cm signal, and in in this paper (which we refer to as Paper II in the following), we focus on evaluating the sensitivity of future 21-cm experiments using this method. As we discussed in Paper I, measurement of statistical anisotropy in the 21-cm signal from the Dark Ages has intrinsic sensitivity to magentic fields in the IGM more than *10 orders of magnitude below the current upper limits from the CMB*. In the following, we demonstrate that a square-kilometer array of dipole antennas in an optimal configuration for cosmological observations (tight tiling of the coverage area with antennas) can reach the sensitivity necessary to detect large-scale magnetic fields that are on the order of 10^{-21} Gauss at $z \sim 20$.

The rest of this paper is organized as follows. In §II, we present a quick overview of the main results in Paper I. In §III, we lay out our notational conventionad and cover the basics of the 21-cm signal and its measurement. In §IV, we derive minimum-variance estimators for a uniform and stochastic magnetic field. In §V, we set up the Fisher analysis formalism necessary to evaluate detectability. In §VI, we present numerical results, and we conclude in §VII. Supporting materials are presented in the appendicies.

II. SUMMARY OF THE METHOD

Magnetic moments of hydrogen atoms in the excited state of the 21-cm line transition tend to be aligned with the incident quadrupole of the 21-cm radiation from the surrounding medium. This effect of "ground-state alignment" [30, 31] arises in a cosmological setting due to velocity-field gradients. In the presence of an external magnetic field, the emitted 21-cm quadrupole is misaligned with the incident quadrupole, due to atomic precession (illustrated in Figure 1). The resulting emission anisotropy can thus be used to trace magnetic fields at high redshifts.

The main result of Paper I was a calculation of the 21-cm brightness-temperature T fluctuation as a function of the line-of-sight direction $\widehat{\mathbf{n}}$, in the frame of the emitting

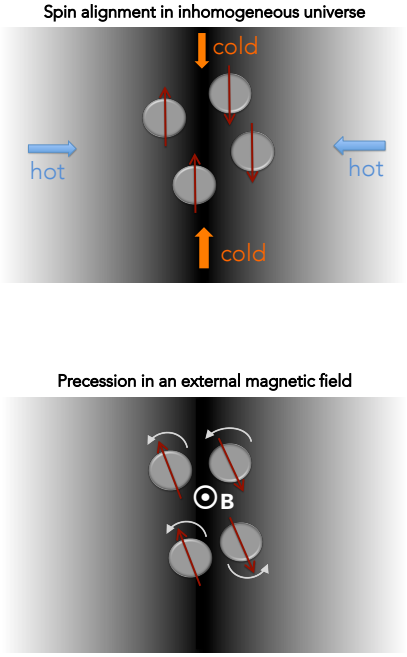

Figure 1. Illustration of the effect of a magnetic field on hydrogen atoms in the excited state of 21-cm transition at high redshifts. In the classical picture, magnetic moments of the atoms (depicted as red arrows) tend to be aligned with density gradients (upper panel; the gradient is depicted with the background shading), unless they precess about the direction of ambient magnetic field (pointing out of the page on the lower panel). When the precessing atoms decay back into the ground state, the emitted quadrupole (aligned with the direction of the magnetic moments) is misaligned with the incident quadrupole. This offset can be observed as a statistical anisotropy in 21-cm brightness-temperature signal, and used to trace cosmological magnetic fields.

ensamble of atoms. The relevant expression is

$$T(\widehat{\mathbf{n}},\widehat{\mathbf{k}}) = \left(1-\frac{T_\gamma}{T_{\rm s}}\right) x_{1{\rm s}} \left(\frac{1+z}{10}\right)^{1/2} \times\Bigg[26.4\ {\rm mK}\Big\{1+\left(1+(\widehat{\mathbf{k}}\cdot\widehat{\mathbf{n}})^2\right)\delta\Big\} - 0.128\ {\rm mK}\left(\frac{T_\gamma}{T_{\rm s}}\right) \times x_{1{\rm s}}\left(\frac{1+z}{10}\right)^{1/2}\Big\{1+2\left(1+(\widehat{\mathbf{k}}\cdot\widehat{\mathbf{n}})^2\right)\delta - \frac{\delta}{15}\sum_m \frac{4\pi}{5}\frac{Y_{2m}(\widehat{\mathbf{k}})\,[Y_{2m}(\widehat{\mathbf{n}})]^*}{1+x_{\alpha,(2)}+x_{{\rm c},(2)}-imx_{\rm B}}\Big\}\Bigg], \tag{1}$$

where the magnetic field is along the z-axis; $x_{\alpha,(2)}$, $x_{{\rm c},(2)}$ and $x_{\rm B}$ parametrize the rates of depolarization of the ground state by optical pumping, atomic collisions, and magnetic precession (relative to radiative depolarization), respectively (defined in detail in Paper I). Furthermore, $T_{\rm s}$ and T_γ are the spin temperature and the CMB temperature at redshift z, respectively; $\widehat{\mathbf{k}}$ is a unit vector in the direction of the wave-vector $\vec{k}$ of a given density Fourier mode; and Y_{2m} represent the usual spin-zero spherical harmonics. Figure 2 illustrates the effect of the magnetic field on the brightness temperature emission pattern in the frame of the atom; shown are quadrupole patterns corresponding to the sum-term of Eq. (1), for various strengths of the magnetic field. Notice that there is a saturation limit for the field strength—in a strong field, the precession is much faster than the decay of the excited state and the emission pattern assymptotes to the one shown in the bottom panel of Figure 2. Above this limit, linear theory breaks down, implying that the signal cannot be used to reconstruct the strength of the field in that regime; however, it is still possible to distinguish saturated regime from the case of no magnetic field, as we will see in §V.

The affect of quadrupole misalignement arises at second order in optical depth (it is a result of a two-scattering process), and is thus a small correction to the total brightness temperature. However, owing to the long lifetime of the excited state (during which even an extremely slow precession has large cumulative effect on the direction of the quadrupole at second order), the effect of misalignement is excuisitively sensitive to magnetic fields in the IGM at redshifts prior to cosmic reionization. As we showed in Paper I, a miniscule magnetic field of 10^{-21} Gauss (in comoving units) produces order-one changes in the direction of the quadrupole. This means that a high-precision measurement of the 21-cm brightness-temperature 2-point correlation function intrinsically has that level of sensitivity to detecting magnetic fields in the Dark Ages. We now proceed to develop a formalism to search for this effect with surveys of redshifted 21-cm line, and to identifying experimental setups that can achieve this goal.

III. BASICS

Before focusing on the estimator formalism in the next Section, here we review the basics of 21-cm brightness temperature fluctuation measurements. In §III A, we setup our notation and review definitions of quantities describing sensitivity of interferometric radio arrays; in §III B, we focus on the derivation of the noise power spectrum; and in §III C, we discuss the effects of the array configuration and its relation to coverage of modes in the uv plane.

A. Definitions

The redshifted 21-cm signal can be represented with specific intensity at a location in physical space $I(\vec{r})$ or in Fourier space $\widetilde{I}(\vec{k})$. In sky coordinates (centered on an emitting patch of the sky), these functions become $\mathcal{I}(\theta_x,\theta_y,\theta_\nu)$ and $\widetilde{\mathcal{I}}(u,v,\eta)$, respectively. Here, vector $\vec{k}$

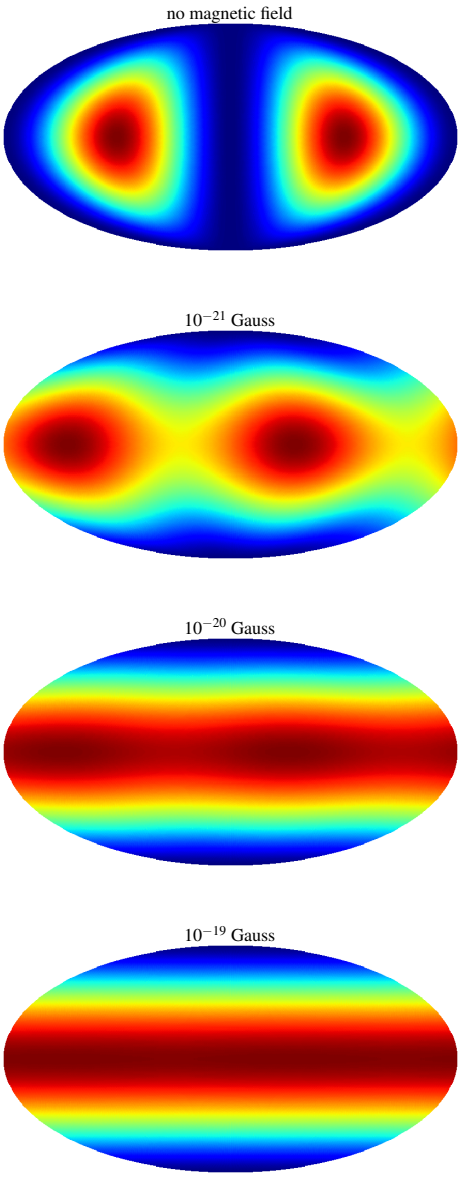

Figure 2. Illustration of the quadrupolar pattern of 21-cm emission from the last (B-dependent) term of Eq. (1) in the frame of the emitting atoms, for the case where $\vec{k}$ is perpendicular to $\hat{\mathbf{n}}$ (maximal signal), shown in Molleweide projection. Lower panels correspond to increasingly stronger magnetic fields (strength denoted on each panel in comoving units), with the bottom panel corresponding to the saturated case. Notice how the type of quadrupole in the top panel ("weak field" regime) is distinct from that in the bottom panel ("strong field" regime).

(in the units of comoving Mpc^{-1}) is a Fourier dual of $\vec{r}$ (comoving Mpc), and likewise, θ_x (rad), θ_y (rad), and θ_ν (Hz) are duals of the coordinates u (rad^{-1}), v (rad^{-1}), and η (seconds), respectively. Notice that θ_x and θ_y represent the angular extent of the patch in the sky, while θ_ν represents its extent in frequency space. The two sets of coordinates are related through linear transformations in the following way

$$\begin{aligned} \theta_x &= \frac{r_x}{\chi(z)}, & u &= \frac{k_x \chi(z)}{2\pi}, \\ \theta_y &= \frac{r_y}{\chi(z)}, & v &= \frac{k_y \chi(z)}{2\pi}, \\ \theta_\nu &= \frac{H(z)\nu_{21}}{c(1+z)^2} r_z, & \eta &= \frac{c(1+z)^2}{2\pi H(z)\nu_{21}} k_z, \end{aligned} \tag{2}$$

where ν_{21} is the 21-cm frequency in the rest frame of emitting atoms, $H(z)$ iz the Hubble parameter, $\chi(z)$ is the comoving distance to redshift z, which marks the middle of the observed data cube (where r_z and θ_ν intervals are evaluated). Note that $2\pi\theta_i u = r_i k_i$, for $i \in \{x, y\}$. The convention we use for the Fourier transforms is

$$\begin{aligned} I(\vec{r}) &= \frac{1}{(2\pi)^3} \int \widetilde{I}(\vec{k}) e^{i\vec{k}\cdot\vec{r}} d\vec{k}, \\ \widetilde{I}(\vec{k}) &= \int I(\vec{r}) e^{-i\vec{k}\cdot\vec{r}} d\vec{r}, \end{aligned} \tag{3}$$

where Fourier-space functions are denoted with tilde. Similarly,

$$\begin{aligned} \mathcal{I}(\theta_x, \theta_y, \theta_\nu) &= \int \widetilde{\mathcal{I}}(u, v, \eta) e^{2\pi i(u\theta_x + v\theta_y + \eta\theta_\nu)} du dv d\eta, \\ \widetilde{\mathcal{I}}(u, v, \eta) &= \int \mathcal{I}(\theta_x, \theta_y, \theta_\nu) e^{-2\pi i(u\theta_x + v\theta_y + \eta\theta_\nu)} d\theta_x d\theta_y d\theta_\nu. \end{aligned} \tag{4}$$

From Eqs. (2)–(4), we can see that the following scaling relation is saticefied

$$\widetilde{I}(\vec{k}) = \frac{c(1+z)^2 \chi(z)^2}{H(z)\nu_{21}} \widetilde{\mathcal{I}}(u, v, \eta), \tag{5}$$

where the proportionallity factor contains the transformation Jacobian $\frac{dr_x dr_y dr_z}{d\theta_x d\theta_y d\theta_\nu}$. Finally, the relationship between the specific intensity in the uv-plane and the visibility function $V(u, v, \theta_\nu)$ is given by the Fourier transform of the frequency coordinate,

$$\begin{aligned} V(u, v, \theta_\nu) &= \int \widetilde{\mathcal{I}}(u, v, \eta) e^{2\pi i \theta_\nu \eta} d\eta, \\ \widetilde{\mathcal{I}}(u, v, \eta) &= \int V(u, v, \theta_\nu) e^{-2\pi i \theta_\nu \eta} d\theta_\nu. \end{aligned} \tag{6}$$

Here, $\theta_{\nu,\max} - \theta_{\nu,\min} = \Delta\nu$ is the bandwidth of the observed data cube centered on z (see also Appendix A).

B. Power spectra and noise

In this Section, we derive the noise power spectrum for the brightness temperature signal. We start by defining a brightness-temperature power spectrum as

$$\langle \widetilde{I}(\vec{k}) \widetilde{I}^*(\vec{k}') \rangle \equiv (2\pi)^3 P_{\widetilde{I}} \delta_D(\vec{k} - \vec{k}'), \tag{7}$$

where δ_D is Dirac delta function. The observable quantity of the interferometric arrays is the visibility function—a complex Gaussian variable with a zero mean and the following variance (derived in Appendix A)

$$\begin{aligned}&\langle V(u,v,\theta_\nu)V(u',v',\theta'_\nu)^*\rangle\\&=\frac{1}{\Omega_{\rm beam}}\left(\frac{2k_BT_{\rm sky}}{A_e\sqrt{\Delta\nu t_1}}\right)^2\delta_D(u-u')\delta_D(v-v')\delta_{\theta_\nu\theta'_\nu},\end{aligned}\tag{8}$$

where $T_{\rm sky}$ is the sky temperature (that includes both the foreground signal from the Galaxy, and the instrument noise); t_1 is the total time a single baseline observes element (u,v) in the uv plane; A_e is the collecting area of a single dish; k_B is the Boltzmann constant; $\Delta\nu$ is the bandwidth of a single observation centered on z; and the last δ in this expression denotes the Kronecker delta.

In the next step, we to combine Eqs. (6) and (8), and take the ensamble average,

$$\begin{aligned}&\langle\widetilde{\mathcal{I}}(u,v,\eta)\widetilde{\mathcal{I}}^*(u',v',\eta')\rangle\\&=\frac{1}{t_1\Omega_{\rm beam}}\left(\frac{2k_BT_{\rm sky}}{A_e}\right)^2\delta_D(u-u')\delta_D(v-v')\delta_D(\eta-\eta'),\end{aligned}\tag{9}$$

where we used

$$\int e^{2\pi i\theta_\nu(\eta-\eta')}d\theta_\nu=\delta_D(\eta-\eta').\tag{10}$$

Taking into account the scaling relation of Eq. (5), using Eq. (7), and keeping in mind the scaling property of the delta function, we arrive at

$$P_1^N(\vec{k})=\frac{c(1+z)^2\chi^2(z)}{\Omega_{\rm beam}t_1H(z)\nu_{21}}\left(\frac{2k_BT_{\rm sky}}{A_e}\right)^2,\tag{11}$$

for the noise power per $\vec{k}$ mode, per baseline.

In the last step, we wish to get from Eq. (11) to the expression for the noise power spectrum that corresponds to observation with all available baselines. To do that, we need to incorporate information about the array configuration and its coverage of the uv plane. In other words, we need to divide the expression in Eq. (11) by the number density of baselines $n_{\rm base}(\vec{k})$ that observe a given mode $\vec{k}$ at a given time (for a discussion of the uv coverage, see the following Section). The final result for the noise power spectrum per mode $\vec{k}$ in the intensity units is

$$P^N(\vec{k})=\frac{c(1+z)^2\chi^2(z)}{\Omega_{\rm beam}t_1H(z)\nu_{21}}\frac{(2k_BT_{\rm sky})^2}{A_e^2n_{\rm base}(\vec{k})},\tag{12}$$

and in temperature units

$$P^N(\vec{k})=\frac{\lambda^4c(1+z)^2\chi^2(z)}{\Omega_{\rm beam}t_1H(z)\nu_{21}}\frac{T_{\rm sky}^2}{A_e^2n_{\rm base}(\vec{k})},\tag{13}$$

where $\lambda=c/\nu_{21}(1+z)$.

C. The UV coverage

Total number density $n_{\rm base}(\vec{k})$ of baselines that can observe mode $\vec{k}$ is related to the (unitless) number density $n(u,v)$ of baselines per $dudv$ element as

$$n_{\rm base}(\vec{k})=\frac{n(u,v)}{\Omega_{\rm beam}},\tag{14}$$

where $\frac{1}{\Omega_{\rm beam}}$ represents an element in the uv plane. The number density integrates to the total number of baselines $N_{\rm base}$,

$$N_{\rm base}=\frac{1}{2}N_{\rm ant}(N_{\rm ant}+1)=\int_{\rm half}n(u,v)dudv,\tag{15}$$

where $N_{\rm ant}$ is the number of antennas in the array, and the integration is done on the half of the uv plane (because the visibility has the following property $V(u,v,\theta_\nu)=V^*(-u,-v,\theta_\nu)$, and only half the plane contains independent samples). We assume that the array consists of many antennas, so that time-dependence of $n(u,v)$ is negligible; if this is not the case, time average of this quantity should be computed to account for Earth's rotation.

In this work, we focus on a specific array configuration that is of particualr interest to cosmology—a tightly packed array of dipole antennas, tiling a surface of the area $(\Delta L)^2$, with a filling fraction close to one. This has been proposed for the Fast Fourier Transform Telescope (FFTT) [32] and is being implemented for Hydrogen Epoch of Reionization Array (HERA) [29], for example. In this case, the beam solid angle is 1 sr, the affective area of a single dipole is $A_e=\lambda^2$, and the effective number of antennas is $N_{\rm ant}=\frac{(\Delta L)^2}{\lambda^2}$. For such configuration, the number density of baselines entering calculation of the noise power spectrum reads

$$n(u,v)=(\frac{\Delta L}{\lambda}-u)(\frac{\Delta L}{\lambda}-v).\tag{16}$$

The relation between $\vec{k}=(k,\theta_k,\phi_k)$ and (u,v) is

$$\begin{aligned}u_\perp&\equiv\frac{\chi(z)}{2\pi}k\sin\theta_k,\\u&=u_\perp\cos\phi_k,\\v&=u_\perp\sin\phi_k,\end{aligned}\tag{17}$$

where subscript $\perp$ denotes components perpendicular to the line-of-sight direction $\widehat{\mathbf{n}}$, which, in this case, is along the z axis. From this, the corresponsing number of baselines observing a given $\vec{k}$ is

$$\begin{aligned}n_{\rm base}(\vec{k})=&(\frac{\Delta L}{\lambda}-\frac{\chi(z)}{2\pi}k\sin\theta_k\cos\phi_k)\\&\times(\frac{\Delta L}{\lambda}-\frac{\chi(z)}{2\pi}k\sin\theta_k\sin\phi_k).\end{aligned}\tag{18}$$

As a last note, when computing numerical results in §VI, we substitute ϕ_k-averaged version of this quantity (between 0 and $\pi/2$ only, due to the four-fold symmetry

of the experimental setup of a square of dipoles) when computing the noise power, in order to account for the rotation of the baselines with respect to the modes. This average number density reads

$$\langle n_{\rm base}(\vec{k})\rangle_{\phi_k} = \left(\frac{\Delta L}{\lambda}\right)^2 - \frac{4}{\pi}\frac{\Delta L}{\lambda}\frac{\chi(z)}{2\pi}k\sin\theta_k + \left(\frac{\chi(z)}{2\pi}k\sin\theta_k\right)^2. \tag{19}$$

IV. QUADRATIC ESTIMATOR FORMALISM

We now derive an unbiased minimum–variance quadratic estimator for a cosmic magnetic field $\vec{B}$, following a formalism similar to what is used in CMB studies [33]. In the following, we assume that the field only evolves (adiabatically) due to the expansion of the universe,

$$B(z) = B_0(1+z)^2, \tag{20}$$

where B_0 is its present–day value (its value in comoving units). The corresponding estimator is denoted with a hat sign, $\widehat{B}_0$. We first consider the case of a field uniform in the entire survey volume; this case is described by a single parameter, B_0. Then we move on to the case of a stochastic magnetic field, with a given power spectrum $P_B(\vec{K})$ (where $\vec{K}$ stands for the wavevector of a given the mode of the field); in this case, the relevant parameter is the amplitude of this power spectrum, A_0^2. In both cases, we assume a separation of scales: density–field modes in consideration must have much smaller wavelength than the coherence scale of the magnetic field (or a given mode wavelength for the case of a stochastic magnetic field), and both length scales must be shorter than the size of the tomography survey at hand.

A. Uniform field

In this Section, we derive an estimator $\widehat{B}_0$ for a comoving uniform magnetic field. We start by noting that the redshifted 21-cm brightness temperature $T(\vec{k})$ contains contributions from the noise $T^N(\vec{k})$ (coming from the instrumental noise plus foregrounds), and the signal $T^S(\vec{k})$ (receiving contributions from the magnetic field, and from the null–case 21-cm signal with no magnetic field, $T_0^S(\vec{k})$),

$$T(\vec{k}) = T^N(\vec{k}) + T^S(\vec{k}),$$
$$T^S(\vec{k}) = T_0^S(\vec{k}) + B_0\frac{\partial T_0^S}{\partial B_0}(\vec{k}), \tag{21}$$

where B is a small expansion parameter (we adopt the linear-theory approach throught this work). We use the subscript "0" to denote functions evaluated at $B = 0$. Temperature is proportional to the density fluctuation δ, with the transfer funtion $G(\widehat{\mathbf{k}})$ as the proportionality factor, such that

$$G(\widehat{\mathbf{k}}) \equiv \frac{\partial T}{\partial\delta}(\widehat{\mathbf{k}}, \delta = 0) \tag{22}$$

and

$$T^S(\vec{k}) = G(\widehat{\mathbf{k}})\delta(k),$$
$$T_0^S(\vec{k}) = G_0(\widehat{\mathbf{k}})\delta(k), \tag{23}$$

where $\widehat{\mathbf{k}} = (\theta_k, \phi_k)$ is a unit vector in the direction of $\vec{k}$. Note that we do not write explicitly dependence of G on z and the cosmological parameters; furthermore, note that G is a function of the direction vector $\widehat{\mathbf{k}}$, while the power spectrum P_δ is a function of the magnitude k, in an isotropic universe. For a magnetic field along the z axis, the explicit expression for the transfer function is derived from Eq. (1) and reads

$$G(\widehat{\mathbf{k}}) = \left(1 - \frac{T_\gamma}{T_{\rm s}}\right) x_{1\rm s}\left(\frac{1+z}{10}\right)^{1/2} \times\Bigg[26.4\ {\rm mK}\left(1 + (\widehat{\mathbf{k}}\cdot\widehat{\mathbf{n}})^2\right) - 0.128\ {\rm mK}\left(\frac{T_\gamma}{T_{\rm s}}\right) \times x_{1\rm s}\left(\frac{1+z}{10}\right)^{1/2}\Big\{2\left(1 + (\widehat{\mathbf{k}}\cdot\widehat{\mathbf{n}})^2\right) - \sum_m \frac{4\pi}{75}\frac{Y_{2m}(\widehat{\mathbf{k}})\left[Y_{2m}(\widehat{\mathbf{n}})\right]^*}{1 + x_{\alpha,(2)} + x_{{\rm c},(2)} - imx_{\rm B}}\Big\}\Bigg], \tag{24}$$

For simplicity of the expressions, we adopt the following notation

$$\frac{\partial T_0^S}{\partial B_0}(\vec{k}) \equiv \delta(k)\frac{\partial G}{\partial B_0}(\widehat{\mathbf{k}}, B_0 = 0),$$
$$\frac{\partial G_0}{\partial B_0}(\widehat{\mathbf{k}}) \equiv \frac{\partial G}{\partial B_0}(\widehat{\mathbf{k}}, B_0 = 0). \tag{25}$$

Since in the rest of this work we assume adiabatic evolution of the magnetic field, it is worth noting that $\frac{\partial G_0}{\partial B_0} = \frac{\partial G_0}{\partial B}(1+z)^2$. Furthermore, we denote the power spectrum in the null case as

$$P_{\rm null}(\vec{k}) \equiv P^N(\vec{k}) + P_0^S(\vec{k}). \tag{26}$$

The signal power spectrum in the absence of a magnetic fields is given as

$$\left\langle T_0(\vec{k})T_0^*(\vec{k}')\right\rangle \equiv (2\pi)^3\delta_D(\vec{k}-\vec{k}')P_0^S(\vec{k}) = (2\pi)^3\delta_D(\vec{k}-\vec{k}')G_0^2(\widehat{\mathbf{k}})P_\delta(k), \tag{27}$$

where

$$\left\langle\delta(\vec{k})\delta^*(\vec{k}')\right\rangle \equiv (2\pi)^3\delta_D(\vec{k}-\vec{k}')P_\delta(k). \tag{28}$$

The observable 2-point correlation function in Fourier space is

$$\begin{aligned}\langle T(\vec{k})T^*(\vec{k}')\rangle &= P_{\rm null}(\vec{k})(2\pi)^3\delta_D(\vec{k}-\vec{k}')\\ +\langle T_0^S(\vec{k})B_0\frac{\partial T_0^{S,*}}{\partial B_0}(\vec{k}')\rangle &+ \langle T_0^{S,*}(\vec{k}')B_0\frac{\partial T_0^S}{\partial B_0}(\vec{k})\rangle\\ &= \left(P_{\rm null}(\vec{k}) + 2B_0P_\delta(k)G_0(\widehat{\mathbf{k}})\frac{\partial G}{\partial B_0}(\widehat{\mathbf{k}})\right)\\ &\times(2\pi)^3\delta_D(\vec{k}-\vec{k}'),\end{aligned} \tag{29}$$

where we assume that the signal and the noise are uncorrelated and keep only terms linear in B_0, and used the reality of G_0 and $\frac{\partial G}{\partial B_0}$.

Since we observe only one universe, the measured proxy for the ensamble average in Eq. (29) is the product $T(\vec{k})T^*(\vec{k})$. Using Eq. (29), each $T(\vec{k})$ gives an estimate for B_0,

$$\widehat{B}_0^{\vec{k}} = \frac{\frac{1}{V}T(\vec{k})T^*(\vec{k}) - P_{\rm null}(\vec{k})}{2P_\delta(k)G_0(\widehat{\mathbf{k}})\frac{\partial G_0}{\partial B_0}(\widehat{\mathbf{k}})}, \tag{30}$$

where we use the following property of the Dirac delta function on a finite volume of the survey V

$$\delta_D(\vec{k}-\vec{k}') = \frac{V}{(2\pi)^3}, \quad \text{for } \vec{k}=\vec{k}', \tag{31}$$

related to the Kroneker delta,

$$\delta_{\vec{k}\vec{k}'} = \frac{(2\pi)^3}{V}\delta_D(\vec{k}-\vec{k}'), \tag{32}$$

and the following normalization convention

$$(2\pi)^3\delta_D(\vec{k}-\vec{k}') \equiv \int d\vec{r}e^{-i\vec{r}\cdot(\vec{k}-\vec{k}')}. \tag{33}$$

The estimator of Eq. (30) is unbiased, $\langle\widehat{B}_0^{\vec{k}}\rangle = 0$. The covariance of the estimates from all available temperature-field modes $\langle\widehat{B}_0^{\vec{k}}\widehat{B}_0^{\vec{k}',*}\rangle$ involves temperature-field 4-point correlation with three Wick constractions; its numerator reads

$$\begin{aligned}&\frac{1}{V^2}\langle T(\vec{k})T^*(\vec{k})T(\vec{k}')T^*(\vec{k}')\rangle + P_{\rm null}(\vec{k})P_{\rm null}(\vec{k}')\\ -\frac{1}{V}P_{\rm null}(\vec{k})\langle T(\vec{k}')T^*(\vec{k}')\rangle &- \frac{1}{V}P_{\rm null}(\vec{k}')\langle T(\vec{k})T^*(\vec{k})\rangle\\ &= P_{\rm null}(\vec{k})P_{\rm null}(\vec{k}')\left[\frac{(2\pi)^6}{V^2}\,\delta_D(\vec{k}-\vec{k})\delta_D(\vec{k}'-\vec{k}')\right.\\ +\frac{(2\pi)^6}{V^2}\delta_D(\vec{k}-\vec{k}')\delta_D(\vec{k}-\vec{k}') &+ \frac{(2\pi)^6}{V^2}\delta_D(\vec{k}+\vec{k}')\delta_D(\vec{k}+\vec{k}')\\ -\frac{(2\pi)^3}{V}\delta_D(\vec{k}'-\vec{k}') &- \left.\frac{(2\pi)^3}{V}\delta_D(\vec{k}-\vec{k})\right]\\ &= P_{\rm null}(\vec{k})P_{\rm null}(\vec{k}')\left(\delta_{\vec{k},\vec{k}'}+\delta_{\vec{k},-\vec{k}'}\right)\end{aligned} \tag{34}$$

where every ensamble average yielded one factor of V. Finally, we get the following expression

$$\langle\widehat{B}_0^{\vec{k}}\widehat{B}_0^{\vec{k}',*}\rangle = \frac{P_{\rm null}^2(\vec{k})\left(\delta_{\vec{k},\vec{k}'}+\delta_{\vec{k},-\vec{k}'}\right)}{4P_\delta(k)^2\left[G_0(\widehat{\mathbf{k}})\frac{\partial G_0}{\partial B_0}(\widehat{\mathbf{k}})\right]^2}, \tag{35}$$

Estimates coming from different $\vec{k}$-modes can be combined with inverse-variance weights in the usual way to form a minimum-variance estimator,

$$\widehat{B}_0 = \frac{\sum_{\vec{k}}\frac{\widehat{B}_0^{\vec{k}}}{\langle\widehat{B}_0^{\vec{k}}\widehat{B}_0^{\vec{k},*}\rangle}}{\sum_{\vec{k}}\frac{1}{\langle\widehat{B}_0^{\vec{k}}\widehat{B}_0^{\vec{k},*}\rangle}}. \tag{36}$$

The final expression for the minimum-variance quadratic estimator computed from temperature measurements at a given redshift is

$$\begin{aligned}\widehat{B}_0 = \sigma^2_{\widehat{B}_0}\sum_{\vec{k}}&\frac{\frac{1}{V}T(\vec{k})T^*(\vec{k}) - P_{\rm null}(\vec{k})}{P_{\rm null}^2(\vec{k})}\\ &\times 2P_\delta(k)G_0(\widehat{\mathbf{k}})\frac{\partial G_0}{\partial B_0}(\widehat{\mathbf{k}}),\end{aligned} \tag{37}$$

with variance given by

$$\sigma^{-2}_{\widehat{B}_0} = \frac{1}{2}\sum_{\vec{k}}\left(\frac{2P_\delta(k)G_0(\widehat{\mathbf{k}})\frac{\partial G_0}{\partial B_0}(\widehat{\mathbf{k}})}{P_{\rm null}(\vec{k})}\right)^2, \tag{38}$$

where the sums are over the whole $\vec{k}$-plane.[1]

B. Stochastic field

We now derive a minimum-variance quadratic estimator for Fourier modes of a stochastic magnetic field. Note that in this Section we do *not* assume a particular model for its power spectrum. We use B_0 to denote a component of the magnetic field along one of the three Cartesian-system axes, and $\vec{r}$ to denote a position vector in physical space. We start with

$$T(\vec{r}) = T_0^S(\vec{r}) + B_0(\vec{r})\frac{\partial T_0^S}{\partial B_0}(\vec{r}), \tag{39}$$

where the subscripts and superscripts have the same meaning as before. Note that the distinction from the

[1] Note that $\widehat{B}_0^{\vec{k}} = \widehat{B}_0^{-\vec{k}}$, following from the reality condition on the temperature field, $T(\vec{k}) = T^*(-\vec{k})$, and the isotropy of space in the null-assumption case, $G(\widehat{\mathbf{k}}) = G(-\widehat{\mathbf{k}})$, which is why the factor of 1/2 appears in order to avoid double-counting of modes.

uniform field case is that the components of the magnetic field are now functions of $\vec{r}$. In Fourier space, we have

$$\begin{aligned} T(\vec{k}) &= T_0^S(\vec{k}) + \int d\vec{r} e^{-i\vec{k}\cdot\vec{r}} B_0(\vec{r}) \frac{\partial T_0^S}{\partial B_0}(\vec{r}) \\ &= T_0^S(\vec{k}) + \frac{1}{(2\pi)^3} \int d\vec{k}_1 B_0(\vec{k}_1) \frac{\partial T_0^S}{\partial B_0}(\vec{k} - \vec{k}_1), \end{aligned} \tag{40}$$

where the last step used the convolution theorem.

In this case, the observable 2-point correlation function in Fourier space becomes

$$\begin{aligned} \left\langle T(\vec{k}) T^*(\vec{k}') \right\rangle &= (2\pi)^3 \delta_D(\vec{k} - \vec{k}') P_{\rm null}(\vec{k}) \\ &+ \left\langle T_0^{S,*}(\vec{k}') \frac{1}{(2\pi)^3} \int d\vec{k}_1 B_0(\vec{k}_1) \frac{\partial T_0^S}{\partial B_0}(\vec{k} - \vec{k}_1) \right\rangle \\ &+ \left\langle T_0^S(\vec{k}) \frac{1}{(2\pi)^3} \int d\vec{k}_1 B_0^*(\vec{k}_1) \left(\frac{\partial T_0^S}{\partial B_0}(\vec{k}' - \vec{k}_1) \right)^* \right\rangle, \end{aligned} \tag{41}$$

to first order in B_0. Using Eqs. (23), (25), and (28), we further get

$$\begin{aligned} \left\langle T(\vec{k}) T^*(\vec{k}') \right\rangle &= (2\pi)^3 \delta_D(\vec{k} - \vec{k}') P_{\rm null}(\vec{k}) + B_0(\vec{k} - \vec{k}') \\ &\times \left[P_\delta(k') G_0^*(\widehat{\mathbf{k}}') \frac{\partial G_0}{\partial B_0}(\widehat{\mathbf{k}}') + P_\delta(k) G_0(\widehat{\mathbf{k}}) \frac{\partial G_0^*}{\partial B_0}(\widehat{\mathbf{k}}) \right], \end{aligned} \tag{42}$$

where we also used the reality of the B_0 field that warrants $B_0^*(-\vec{K}) = B_0(\vec{K})$. Now, using a procedure analogous to that presented in §IV A, we can estimate $B_0(\vec{K} \equiv \vec{k} - \vec{k}')$ from $\vec{k}\vec{k}'$ pair of mode measurements in the temperature field as

$$\widehat{B}_0^{\vec{k}\vec{k}'}(\vec{K}) = \frac{T(\vec{k}) T^*(\vec{k}')}{P_\delta(k') G_0^*(\widehat{\mathbf{k}}') \frac{\partial G_0}{\partial B_0}(\widehat{\mathbf{k}}') + P_\delta(k) G_0(\widehat{\mathbf{k}}) \frac{\partial G_0^*}{\partial B_0}(\widehat{\mathbf{k}})}, \tag{43}$$

where we only focus on terms $\vec{K} \neq 0$ ($\vec{k} \neq \vec{k}'$). The variance $\left\langle \widehat{B}_0^{\vec{k}\vec{k}'}(\vec{K}) \left(\widehat{B}_0^{\vec{k}\vec{k}'}(\vec{K}') \right)^* \right\rangle$ of this estimator under the null assumption can we evaluated trivially from the above expression. Finally, from Eq. (43), we can derive the full estimator for the mode $B_0(\vec{K})$, in the usual way—by combining the individual $\widehat{B}_0^{\vec{k}\vec{k}'}(\vec{K})$ estimates with inverse-variance weights, and normalizing appropriately. However, for the purpose of detectability analysis, we are only interested in the variance of that estimator, or equivalently, the noise power spectrum of $\widehat{B}_0$, given by

$$\begin{aligned} (2\pi)^3 \delta_D(\vec{K} - \vec{K}') P_{B_0}^N(\vec{K}) &\equiv \left\langle \widehat{B}_0(\vec{K}) \widehat{B}_0(\vec{K}')^* \right\rangle \\ &= \left(\sum_{\vec{k}} \frac{\left(P_\delta(k') G_0^*(\widehat{\mathbf{k}}') \frac{\partial G_0}{\partial B_0}(\widehat{\mathbf{k}}') + P_\delta(k) G_0(\widehat{\mathbf{k}}) \frac{\partial G_0^*}{\partial B_0}(\widehat{\mathbf{k}}) \right)^2}{2V^2 P_{\rm null}(\vec{k}) P_{\rm null}(\vec{k}')} \right)^{-1}, \end{aligned} \tag{44}$$

with the restriction $\vec{K} = \vec{k} - \vec{k}'$. Factor of 2 in the denominator corrects for double-counting mode pairs since $\widehat{B}_0^{\vec{k}\vec{k}'}(\vec{K}) = \left(\widehat{B}_0^{-\vec{k}-\vec{k}'}(\vec{K}) \right)^*$, and the sum in the above expression is unconstrained. If we only consider diagonal terms $\vec{K} = \vec{K}'$, then the LHS of the above expression becomes equal to $V P_{B_0}^N(\vec{K})$. The explicit expression for the noise power spectrum is then

$$\begin{aligned} P_{B_0}^N(\vec{K}) &= \\ \left(\sum_{\vec{k}} \frac{\left(P_\delta(k') G_0^*(\widehat{\mathbf{k}}') \frac{\partial G_0}{\partial B_0}(\widehat{\mathbf{k}}') + P_\delta(k) G_0(\widehat{\mathbf{k}}) \frac{\partial G_0^*}{\partial B_0}(\widehat{\mathbf{k}}) \right)^2}{2V P_{\rm null}(\vec{k}) P_{\rm null}(\vec{k}')} \right)^{-1}, \end{aligned} \tag{45}$$

Note that only the components of the magnetic field in the plane of the sky have an effect of the observed brightness temperature, and so the above expression represents the noise power spectrum for either one of those two (uncorrelated) components. The noise in the direction along the line of sight can be considered infinite. Finally, note that a similar type of estimator can be written down for the direction of the magnetic field in a given patch of the sky. However, in this work we only focus on the magnitude of the field.

V. FISHER ANALYSIS

We now use the key results of §IV to evaluate expressions for sensitivity of future observations. We first derive the expression for sensitivity to a field uniform in the entire survey volume. We start with the unsatured case, and consider the limit where the field (in the classical picture) produces less than 1 radian of precession at all redshifts of interest, and then move on to the saturated (strong field) limit. Secondly, we derive the expression for sensitivity to detecting a stochastic magnetic field with a scale-independent power spectrum.

A. Uniform field case

For a measurement of the redshifted 21-cm brightness temperature signal at a given z, the sensitivity $\sigma_{\widehat{B}_0}$ to recovering a uniform field B_0 in unsaturated limit is given by Eq. (38). The total sensitivity of a tomorgraphy survey over a range of redshifts is given by

$$\begin{aligned} \sigma_{B_0}^{-2} &= \frac{1}{2} \int dV(z) \frac{k^2 dk d\phi_k \sin\theta_k d\theta_k}{(2\pi)^3} \\ &\times \left(\frac{2 P_\delta(k,z) G_0(\theta_k, \phi_k, z) \frac{\partial G_0}{\partial B_0}(\theta_k, \phi_k, z)}{P^N(k, \theta_k, z) + P_\delta(k,z) G_0^2(\theta_k, \phi_k, z)} \right)^2, \end{aligned} \tag{46}$$

where we transitioned from a sum over $\vec{k}$ modes to an integral, using $\sum_{\vec{k}} \to V \int d\vec{k}/(2\pi)^3$. The integral is per-

formed over the (comoving) volume of the survey of angular size $\Omega_{\rm survey}$ (in steradians) at a given redshift,

$$dV = \frac{c}{H(z)}\chi^2(z)\Omega_{\rm survey}dz, \tag{47}$$

and the integration limits are: $\phi_k \in [0, 2\pi]$; $\theta_k \in [0, \pi]$; and $k \in [2\pi u_{\rm min}/(d_A \sin\theta_k), 2\pi u_{\rm max}/(d_A \sin\theta_k)]$, where $u_{\rm min,max} = \frac{L_{\rm min,\ max}}{\lambda}$ correspond to the maximum and minimum baseline $L_{\rm min}$ and $L_{\rm max}$, respectively. If the survey area is big enough that the flat-sky approximation breaks down, $\sigma^{-2}_{B_0}$ can be computed on small (approximately flat) patch of the size $\Omega_{\rm patch}$, centered on the line of sight, and corrected in the following way to account for the total survey volume [2]

$$\begin{aligned}\sigma^{-2}_{\widehat{B}_0,\ {\rm tot}} &= \frac{\sigma^{-2}_{\widehat{B}_0}}{\Omega_{\rm patch}}\int_0^{\theta_{\rm survey}}\int_0^{2\pi}\cos^2\theta d\theta d\phi \\ &= \frac{\sigma^{-2}_{\widehat{B}_0}\pi}{\Omega_{\rm patch}}\left(\theta_{\rm survey} + \cos\theta_{\rm survey}\sin\theta_{\rm survey}\right).\end{aligned} \tag{48}$$

Let us now consider a field that is strong enough to produce precession by more than a radian in a lifetime of the excited state of the 21-cm transition; this is the saturated-signal case. The brightness-temperature 2-point correlation functions still capture the presence of the field in this case (as illustrated in Figure 2), but it loses sensitivity to recovering its exact magnitude. Ability to distinguish staturated case from zero magnetic field becomes a relevant measure of sensitivity in this case.

To evaluate the sensitivity, we can write the signal power spectrum as a sum of contributions from $B_0 = 0$ and $B_0 \to \infty$ cases,

$$P^S(\vec{k}) = (1-\xi)P^S(\vec{k}, B=0) + \xi P^S(\vec{k}, B\to\infty), \tag{49}$$

and perform the standard Fisher analysis to evaluate sensitivity to recovering parameter ξ,

$$\sigma^{-2}_\xi = \int dV(z)\frac{d\vec{k}}{(2\pi)^3}\left(\frac{\frac{\partial P^S}{\partial\xi}(\vec{k})}{P^N(\vec{k}) + P^S_0(\vec{k}, \xi=0)}\right)^2, \tag{50}$$

where

$$\frac{\partial P^S}{\partial\xi}(\vec{k}) = P^S(\vec{k}, B\to\infty) - P^S(\vec{k}, B=0) \tag{51}$$

involves the following limit of the transfer function, derived from Eq. (24),

$$\begin{aligned}G(\widehat{\mathbf{k}}, B\to\infty) &= \left(1 - \frac{T_\gamma}{T_{\rm s}}\right)x_{1{\rm s}}\left(\frac{1+z}{10}\right)^{1/2} \\ &\times\left[26.4\ {\rm mK}\left(1 + (\widehat{\mathbf{k}}\cdot\widehat{\mathbf{n}})^2\right) - 0.128\ {\rm mK}\left(\frac{T_\gamma}{T_{\rm s}}\right)\right. \\ &\left.\times x_{1{\rm s}}\left(\frac{1+z}{10}\right)^{1/2}\left\{2 + 2(\widehat{\mathbf{k}}\cdot\widehat{\mathbf{n}})^2 - \frac{1}{60}\frac{1-3\cos^2\theta_k}{1 + x_{\alpha,(2)} + x_{c,(2)}}\right\}\right],\end{aligned} \tag{52}$$

in the reference frame where the magnetic field is along the z axis, and the line-of-sight direction is perpendicular to is; when using this expression to derive numerical results in the following Section, we are only interested in this configuration, since we only evaluate detectability of the components of B in the plane of the sky. We interpret σ_ξ as a 1σ sensitivity to *detecting* presence of a strong magnetic field.

B. Stochastic field case

Using Eq. (45) and a procedure analogous to the case of a uniform field, we get the following integral expression for the noise power spectrum of a plane-of-the-sky component of the magnetic field

$$\begin{aligned}\left(P^N_{B_{0,i}}(\vec{K})\right)^{-1} &= \int k^2 dk\sin\theta_k d\theta_k d\phi_k \\ &\times\frac{\left(P_\delta(k')G^*_0(\widehat{\mathbf{k}}')\frac{\partial G_0}{\partial B_i}(\widehat{\mathbf{k}}') + P_\delta(k)G_0(\widehat{\mathbf{k}})\frac{\partial G^*_0}{\partial B_i}(\widehat{\mathbf{k}})\right)^2}{2(2\pi)^3 P_{\rm null}(\vec{k})P_{\rm null}(\vec{k}')},\end{aligned} \tag{53}$$

where $\vec{k}' = \vec{K} - \vec{k}$.

To compute signal-to-noise ratio (SNR) for measuring the amplitude of an arbitrary stochastic-field power spectrum in a given redshift slice z we need to perform a sum over all voxels (3d pixels) in the survey volume at that redshift. A general expression for SNR is

$${\rm SNR}^2 = \frac{1}{2}Tr\left(N^{-1}SN^{-1}S\right), \tag{54}$$

where S and N are the signal and noise matrices. In our case, these are $3N_{\rm voxels}\times 3N_{\rm voxels}$ matrices (there are $N_{\rm voxels}$ voxels in the entire survey, and 3 components of the magnetic field). In the null case, voxels are independent, and so the noise matrix is diagonal, and the signal is captured by the 3d power spectrum of the magnetic field. The voxel-noise variance for measuring a single mode is given by $P^N_{B_{0,i}}(\vec{K}, z)/V_{\rm voxel}(z)$, where $V_{\rm voxel}$ is volume of a given voxel. Summing over voxels and components of the magnetic field with inverse-variance weights, for a single redshift slice, we get SNR as

$$\begin{aligned}{\rm SNR}^2(z) &= \frac{1}{2}\sum_{i\alpha,j\beta}\frac{S^2_{i\alpha,j\beta}}{P^N_{B_{0,i}}(\vec{K}, z)P^N_{B_{0,j}}(\vec{K}, z)}V^2_{\rm voxel} \\ &= \frac{1}{2}\sum_{ij}\int d\vec{r}_\alpha\int d\vec{r}_\beta\frac{\langle B_{0,i}(\vec{r}_\alpha)B_{0,j}(\vec{r}_\beta)\rangle^2}{P^N_{B_{0,i}}(\vec{K}, z)P^N_{B_{0,j}}(\vec{K}, z)},\end{aligned} \tag{55}$$

[2] This accounts for the change in the angle that a uniform magnetic field makes with a line of sight, as the line of sight moves through a large survey area.

where we label voxels with Greek indicies, and, as before, retain Roman indicies for the field components; $\vec{r}_{\alpha/\beta}$ represents the spatial position of a given voxel.

To simplify further calculations, we now only focus on a particular class of magnetic-field models, where most of the power is on largest scales (small $\vec{K}$). In this (squeezed) limit, $\vec{K} \ll \vec{k}$ and thus $\vec{k} \approx \vec{k}'$, such that Eq. (53) reduces to the white noise (independent on $\vec{K}$). The model for the power spectrum is defined through

$$(2\pi)^3\delta_D(\vec{K}-\vec{K}')P_{B_{0,i}B_{0,j}}(\vec{K}) \equiv \left\langle B^*_{0,i}(\vec{K})B_{0,j}(\vec{K}')\right\rangle, \tag{56}$$

which relates to the variance in the transverse component $P_{B_\perp}(\vec{K})$ as

$$P_{B_{0,i}B_{0,j}}(\vec{K}) = (\delta_{ij} - \widehat{K}_i\widehat{K}_j)P_{B_\perp}(\vec{K}), \tag{57}$$

where $\widehat{K}_{i/j}$ is a unit vector along the direction of i/j component. In this discussion, as a concrete model example, we consider a scale–independent (SI) power spectrum,

$$P_{B_\perp}(\vec{K}) = A_0^2/K^3, \tag{58}$$

where the amplitude A_0 is a free parameter (in units of Gauss). Furthermore, if homogeneity and isotropy are satisfied, the integrand in Eq. (55) only depends on the separation vector $\vec{s} \equiv \vec{r}_\beta - \vec{r}_\alpha$. Using this and the squeezed limit assumption gives[3]

$$\begin{aligned}\mathrm{SNR}^2(z) &= \frac{1}{2}\sum_{ij}\frac{dV_{\rm patch}}{(P^N_{B_{0,i}}(z))^2}\int d\vec{s}\,\langle B_{0,}i(\vec{r}_\beta-\vec{s})B_{0,j}(\vec{r}_\beta)\rangle^2 \\ &= \frac{1}{2(2\pi)^3}\sum_{ij}\frac{dV_{\rm patch}}{(P^N_{B_{0,i}}(z))^2}\int d\vec{K}\left(P_{B_{0,i}B_{0,j}}(\vec{K})\right)^2,\end{aligned} \tag{59}$$

where $dV_{\rm patch}$ is the volume of a redshift–slice patch of Eq. (47). Substituting Eq. (58), and integrating over all z's available in the survey, total SNR reads

$$\begin{aligned}\mathrm{SNR}^2 = \frac{A_0^4}{2(2\pi)^3}\int_{z_{\rm min}}^{z_{\rm max}}\frac{dV_{\rm patch}}{(P^N_{B_{0,i}}(z))^2}\int_0^\pi \sin\theta d\theta \\ \int_0^{2\pi}d\phi\int_{K_{\rm min}(z,\theta,\phi)}^{K_{\rm max}(z,\theta,\phi)}\frac{dK}{K^4}\sum_{ij\in\{xx,xy,yx,yy\}}(\delta_{ij}-\widehat{K}_i\widehat{K}_j)^2,\end{aligned} \tag{60}$$

where x and y denote components in the plane of the sky, and

$$\widehat{K}_x = \sin\theta\sin\phi,\ \ \widehat{K}_y = \sin\theta\cos\phi. \tag{61}$$

The sum in the above expression reduces to

$$\sum_{ij\in\{xx,xy,yx,yy\}}(\delta_{ij}-\widehat{K}_i\widehat{K}_j)^2 = 2\cos^2\theta + \sin^4\theta. \tag{62}$$

[3] Note that in the last step we used $\int d\vec{s}|f(\vec{s})|^2 = \int\frac{d\vec{K}}{(2\pi)^3}|\widetilde{f}(\vec{K})|^2$, which holds for an arbitrary function f and its Fourier transform $\widetilde{f}$.

Substituting this into Eq. (60), and integrating over K, θ, ϕ gives

$$\mathrm{SNR}^2 = \frac{A_0^4}{10\pi^2}\int_{z_{\rm min}}^{z_{\rm max}}\frac{dV_{\rm patch}}{(P^N_{B_{0,i}}(z))^2}\left(\frac{1}{K^3_{\rm min}}-\frac{1}{K^3_{\rm max}}\right). \tag{63}$$

From this expression, 1σ sensitivity to measuring A_0^2 is

$$\sigma^2_{A_0^2} = \left[\frac{1}{10\pi^2}\int_{z_{\rm min}}^{z_{\rm max}}\frac{dV_{\rm patch}}{(P^N_{B_{0,i}}(z))^2}\left(\frac{1}{K^3_{\rm min}}-\frac{1}{K^3_{\rm max}}\right)\right]^{-1}. \tag{64}$$

VI. RESULTS

We now proceede to numerically evaluate the sensitivity of a tomographic 21-cm survey to detecting magnetic fields during the pre-reionization epoch, using the formalism of previous two Sections. For the purposes of deriving numerical results, we only focus on one type of experimental setup—an array of closely-packed dipole antennas, such as the FFTT considered in §III C. The motivation for this choice is the fact that such configuration is known to maximize sensitivity of cosmological measurements [32]. We consider an array with a surface area of $(\Delta L\ \mathrm{km})^2$ covered in dipole antennas.

The computation of t_1 from the total duration of the survey $t_{\rm obs}$ depends on the type of the experiment. For a beam of a solid angle $\Omega_{\rm beam} = \lambda^2/A_e$ much smaller than the solid angle $\Omega_{\rm survey}$ of the entire survey, where telescopes scan the sky one beamwidth at a time (such as the case for radio dishes), t_1 is the total time spent observing one (u,v) element of size corresponding to the beam size, $t_1 = t_{\rm obs}\Omega_{\rm survey}/\Omega_{\rm beam}$. However, in the case of an array of dipoles, the beam is greater or equal to the survey angular size, and $t_1 = t_{\rm obs}$. When deriving numerical results, we assume the latter. Also, we do not account for the fact that a given patch of the sky is only visible for a part of a day from a given location; therefore, $t_{\rm obs}$ we use in §VI will be shorter than the wall-clock time of the survey, by a factor of a few. We take $\Omega_{\rm survey} = 1$sr, and the wall-clock survey duration of about 2 years (corresponding to $t_1 = 1$ year).For the sky temperature that enters the calculation of the noise power spectrum in Eq. (13), we assume a simple model of Galactic foregrounds from [34], where

$$T_{\rm sky} = 60\left(\frac{21}{100}(1+z)\right)^{2.55}\ [\mathrm{K}]. \tag{65}$$

Furthermore, we assume that the redshift range covered by the survey is $z \in [15, 35]$.

Other ingredients entering the sensitivity calculation are the Lyman-α flux $J_{\rm Ly\alpha}(z)$, and the spin and kinetic temperatures of the IGM; these are obtained using `21CMFAST` [35], for standard cosmology, and are shown in Figure 3. We checked that the variation in the x-ray heating rate within a factor of a few from the fiducial model

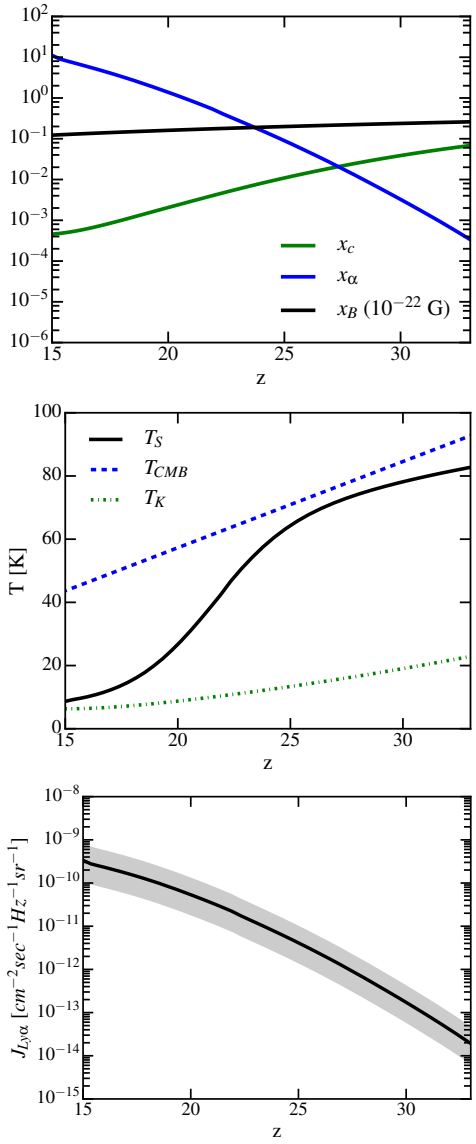

Figure 3. Inputs for sensitivity calculations: Lyman-α flux model, and the relevant spin- and kinetic- temperature models.

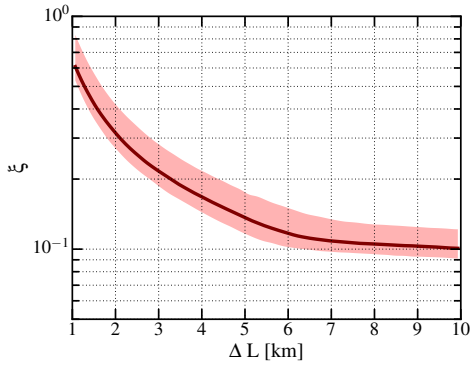

Figure 4. FFTT sensitivity to distinguishing saturated case from no magnetic field (upper panel), as a function of maximum array baseline, assuming a survey size of 1 sr, for survey duration of 2 years.

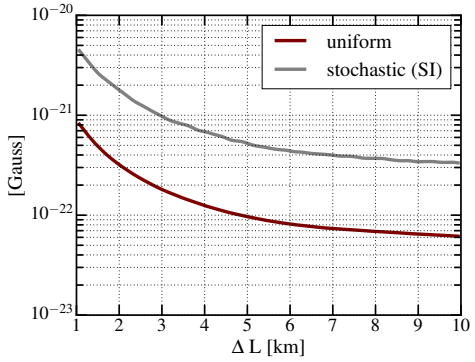

Figure 5. FFTT sensitivity to detecting a uniform and stochastic magnetic field (stochastic field is assumed to have a scale-independent (SI) power spectrum, and shown is the rms per $logK$, A_0/π.), as a function of maximum array baseline, assuming a survey size of 1 sr, for survey duration of 2 years.

does not make significant changes to the presented results. Figures 4 and 5 show how the sensitivity changes as a function of the maximum baseline ΔL (since different baselines may correspond to different stages of the experiment). Figure 4 shows 1σ sensitivity to measuring parameter ξ of Eq. (49), that distinguishes amongst the zero magnetic field case and the case where the field is strong enough that the signal saturates (in the sense described in §II). This parameter is by definition boud between the values of 0 and 1, where 0 represents the case of no magnetic field, and 1 represents the saturated case. From this Figure, we can see that, for example, a little over a square kilometer of covarega area is necessary for a 1σ detection of magnetic fields stronger than about 10^{-21} Gauss comoving. While this size of a radio array is still futuristic in terms of the shear number of antennas (compare to the SKA [27], for example), the number of mode measurements required for this measurement corresponds to the computational demands for the next-generation 21-cm cosmology experiment, and may thus be feasible in the coming couple of decades.

Figure 5 is obtained by evaluating the expressions of Eqs. (46) and (63), and shows sensitivity to measuring the scaled value of the magnetic field in the case of a uniform field (dark red line), and the sensitivity to measuring the amplitude of a particular model for a stochastic field (gray line)—the scale-independent (SI) power spectrum discussed in §V. While the numerical calculation behind this plot assumed that the brightness temperature is a linear function of the field strength, this assumption is not guaranteed to hold—it breaks in the saturation limit, as discussed in §II. In order to understand how the constraints (or, sensitivities) of Figure 5 compare to the saturation "ceiling" at the redshifts we integrate over, we present a rough calculation of the saturation as a function of redshift, and compare it to the values of

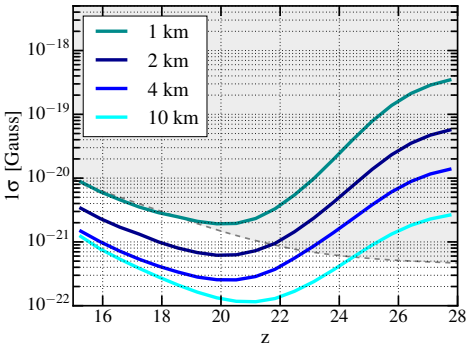

Figure 6. Saturation ceiling is shown as a shaded gray area, and integrand of Eq. (46) (inverse sqare root of it) is shown as a function of redshift, for several maximum baseline sizes. When the colored curves are below the saturation limit around their minima, the analysis assuming unsaturated regime is valid.

the z-dependent integrands of Eq. (46). From this Figure, we can see that only above the coverage of about 16km^2 are we able to actually measure the exact value of the amplitude of the magnetic field power spectrum.

VII. CONCLUSIONS

In Paper I of this series, we proposed a new method to detect extremely weak magnetic fields in the IGM during the Dark Ages, using future 21-cm tomography experiments. In this paper, Paper II, we investigated sensitivity of future radio arrays using this method. We developed minimum-variance-estimator formalism that uses 2-point correlation function of the 21-cm brightness temperature to detect and measure magnetic fields in pre-reionization epoch.

Our results imply that the next-stage array with a little over a square kilometer of area covered in dipole antennas ina tightly-packed configuration, observing redshifts from 15 to 35, can in principle reach the sensitivity to detect magnetic fields on the order of 10^{-21} Gauss comoving. However, disentangling teh exact spectral shape of a stochastic field is more challenging, and can only be expected in the futuristic scenarios where arrays grow to a size of tens of square kilometers in coverage area. In this analysis, we took into account the noise arising from the presence of the large Galactic foreground signal, but we ignotered more subtle effects such as, for example, frequency dependence of the beams, etc., calculation of which would be necessary to create figures of merit for future experiements.

At the end, we emphasize again that the main limitation to sensitivity of this method to measuring magnetic fields at high redshifts is a mere fact that it is based on a two-scattering process—as soon as quality of the 21-cm statistics reaches the levels necessary to probe second-order processes, the effect we focused on in this series of papers will immediately open up an "*in situ*" way to trace miniscule (and possibly primordial) magnetic fields with unprecedented precision.

ACKNOWLEDGMENTS

VG gratefully acknowledges the support from the W. M. Keck Foundation Fund. Illustrations in Figure 2 made use of HEALPix [36] software package[4].

Appendix A: Visibility-variance derivation

Here we derive the variance of the visibility for an interferometric array of two antennas separated by a baseline $\vec{b} = (b_x, b_y)$, each with an effective collecting area A_e, observing a single element in uv plane for time duration t_1, in the total bandwidth $\Delta\nu = \nu_{\rm max} - \nu_{\rm min}$. This setup is shown in Figure 7. Note that modes with frequencies that differ by less than $1/t_1$ cannot be distinguished in observation time t_1, and modes with frequencies in each interval of size $1/t_1$ are "collapsed" into a discrete mode with $\nu_n = n/t_1$, where $n \in Z$. Thus, the number of measured (discrete) frequencies is $N_\nu = t_1\Delta\nu$.

Electric field induced in a single antenna is

$$E(t) = \sum_n^{N_\nu} \widetilde{E}(\nu_n) e^{2\pi i \nu_n t}, \tag{A1}$$

while the quantity an interferometer measures is the correlation coefficient between the electric field in one, E_i, and the electric field in the other antenna, E_j, as a function of frequency,

$$\rho_{ij}(\nu) \equiv \frac{\langle \widetilde{E}_i^*(\nu)\widetilde{E}_j(\nu)\rangle}{\sqrt{\langle|\widetilde{E}_i(\nu)|^2\rangle\langle|\widetilde{E}_j(\nu)|^2\rangle}}. \tag{A2}$$

Let us now assume that

$$\langle \widetilde{E}_i^*(\nu_n)\widetilde{E}_j(\nu_m)\rangle = \sigma(\nu)^2\delta_{mn}, \tag{A3}$$

In the following, for clarity, we will omit writing the explicit dependence on ν. The real (or imaginary) part of ρ has the following variance

$$var(Re[\rho_{ij}])\frac{1}{2N_\nu} = \frac{1}{2t_1\Delta\nu}. \tag{A4}$$

Before continuing, let us take a brief digression to show that the above formula implicitly assumes that the electric fields in the two antennas $\widetilde{E}_i$ and $\widetilde{E}_j$ have a very weak correlation, $\rho \ll 1$. Namely, suppose x and y are random Gaussian variables with zero mean values, where

[4] `http://healpix.sf.net`; `https://github.com/healpy/healpy`

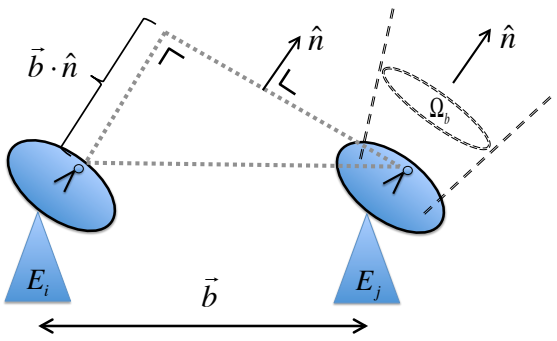

Figure 7. Schematic of a two-antenna interferometer.

$var(x) \equiv \langle (x - \langle x \rangle)^2 \rangle = \langle x^2 \rangle - \langle x \rangle^2 = \langle x^2 \rangle$, and similarly for y, and their correlation coefficient is $\rho \equiv \frac{\langle xy \rangle}{\sqrt{\langle x^2 \rangle \langle y^2 \rangle}}$. In this case, the following is true

$$\begin{aligned} var(xy) &= \langle x^2 y^2 \rangle - \langle xy \rangle^2 = \langle x^2 \rangle \langle y^2 \rangle + \langle xy \rangle^2 \\ &= \langle x^2 \rangle \langle y^2 \rangle + \rho^2 \langle x^2 \rangle \langle y^2 \rangle = var(x) var(y)(1 + \rho^2), \end{aligned} \tag{A5}$$

so that when ρ is small $var(xy) = var(x)var(y)$, which was assumed in the first equality of Eq. (A4).

Resuming the derivation, if different frequencies are uncorrelated, the result of Eq. (A4) implies

$$\langle |\rho_{ij}(\nu)|^2 \rangle = \frac{1}{t_1 \Delta\nu}. \tag{A6}$$

The final step in this derivation requires the relation between intensity in the sky $\mathcal{I}(\theta_x, \theta_y, \nu)$ (within the beam of the solid angle $\Omega_{\rm beam}$, centered on the direction $\hat{\mathbf{n}} = (\theta_x, \theta_y)$) and the electric fields measured in the two antennas,

$$\begin{aligned} \langle \widetilde{E}_i^*(\nu) \widetilde{E}_j(\nu) \rangle \propto \int_{\Omega_{\rm beam}} d\theta_x d\theta_y \mathcal{I}(\theta_x, \theta_y, \theta_\nu) \\ \times e^{i \frac{2\pi\nu}{c}(b_x\theta_x + b_y\theta_y)} R(\theta_x, \theta_y), \end{aligned} \tag{A7}$$

where $R(\theta_x, \theta_y)$ is the antenna response function (the shape of the beam in the sky), which we will assume to be unity. Furthermore, $\frac{2\pi\nu}{c}(b_x\theta_x + b_y\theta_y) \equiv 2\pi(u\theta_x + v\theta_y)$ is the phase delay between two antennae (position in the uv plane measures the phase lag between the two dishes in wavelenghts). The coefficient of proportionallity in the above equation is set by various instrumental parameters, and is not relevant for our purposes. From Eq. (A2), it follows

$$\rho_{ij}(\nu) = \frac{\int_{\Omega_{\rm beam}} d\theta_x d\theta_y \mathcal{I}(\theta_x, \theta_y, \theta_\nu) e^{2\pi i(u\theta_x + v\theta_y)}}{\int_{\Omega_{\rm beam}} d\theta_x d\theta_y \mathcal{I}(\theta_x, \theta_y, \theta_\nu)}, \tag{A8}$$

where the denominator in the above formula approximately integrates to (for a small beam)

$$\int_{\Omega_{\rm beam}} d\theta_x d\theta_y \mathcal{I}(\theta_x, \theta_y, \theta_\nu) \approx \Omega_{\rm beam} \mathcal{I}(\theta_x, \theta_y, \theta_\nu). \tag{A9}$$

We can now use the approximate expression for the resolution of a single dish,

$$\Omega_{\rm beam} = \frac{\lambda^2}{A_e}, \tag{A10}$$

the Reyliegh-Jeans law (or the definition of the brightness temperature),

$$\mathcal{I}(\theta_x, \theta_y, \theta_\nu) = \frac{2k_B T_{\rm sky}}{\lambda^2}, \tag{A11}$$

and note that the numerator in Eq. (A8) matches the definition of visibility from Eq. (6) to get

$$\rho_{ij}(\nu) = \frac{A_e}{2k_B T_{\rm sky}} V(u, v, \theta_\nu), \tag{A12}$$

Combining the above expression and Eq. (A6), we get the final result of this derivation,

$$\begin{aligned} \langle |V(u, v, \theta_\nu)|^2 \rangle = \frac{1}{\Omega_{\rm beam}} \left(\frac{2k_B T_{\rm sky}}{A_e \sqrt{t_1 \Delta\nu}} \right)^2 \\ \times \delta_D(u - u') \delta_D(v - v') \delta_{\theta_\nu \theta_{\nu'}}, \end{aligned} \tag{A13}$$

where V is a complex Gaussian variable, centered at zero, and uncorrelated for different values of its arguments, and the factor of $\Omega_{\rm beam}$ came from converting from Kroneker to Dirac deltas.

It should be noted at the end that we were calculating the contribution to the visibility from the noise only (the system + the foregrounds in the absence of a signal), so we used system temperature for brightness temperature (this could contain the signal from foregrounds and from the instrument). In case we want to repeat the computation in the presence of a signal, $T_{\rm sky}$ should instead be the sum of the signal and the noise temperatures.

[1] R. Durrer and A. Neronov, Astron. and Astrophys. Review **21**, 62 (2013), arXiv:1303.7121 [astro-ph.CO].

[2] J. P. Vallee, New Astronomy Reviews **48**, 763 (2004).

[3] A. Neronov and I. Vovk, Science **328**, 73 (2010), arXiv:1006.3504 [astro-ph.HE].

[4] R. Wielebinski, in *Cosmic Magnetic Fields*, Lecture

Notes in Physics, Berlin Springer Verlag, Vol. 664, edited by R. Wielebinski and R. Beck (2005) p. 89.
[5] R. Beck, Space Science Reviews **166**, 215 (2012).
[6] K. Park, E. G. Blackman, and K. Subramanian, Phys. Rev. E **87**, 053110 (2013), arXiv:1305.2080 [physics.plasm-ph].
[7] S. Naoz and R. Narayan, Physical Review Letters **111**, 051303 (2013), arXiv:1304.5792 [astro-ph.CO].
[8] S. Naoz and R. Narayan, Physical Review Letters **111**, 051303 (2013), arXiv:1304.5792 [astro-ph.CO].
[9] L. M. Widrow, D. Ryu, D. R. G. Schleicher, K. Subramanian, C. G. Tsagas, and R. A. Treumann, Space Science Reviews **166**, 37 (2012), arXiv:1109.4052 [astro-ph.CO].
[10] T. Kobayashi, Journal of Cosmology and Astroparticle Physics **5**, 040 (2014), arXiv:1403.5168.
[11] D. G. Yamazaki, K. Ichiki, T. Kajino, and G. J. Mathews, Advances in Astronomy **2010** (2010), arXiv:1112.4922 [astro-ph.CO].
[12] P. Blasi, S. Burles, and A. V. Olinto, Astrophysical Journal, Letters **514**, L79 (1999), astro-ph/9812487.
[13] F. Tavecchio, G. Ghisellini, L. Foschini, G. Bonnoli, G. Ghirlanda, and P. Coppi, MNRAS **406**, L70 (2010), arXiv:1004.1329 [astro-ph.CO].
[14] K. Dolag, M. Kachelriess, S. Ostapchenko, and R. Tomàs, Astrophysical Journal, Letters **727**, L4 (2011), arXiv:1009.1782 [astro-ph.HE].
[15] K. E. Kunze and E. Komatsu, Journal of Cosmology and Astroparticle Physics **1**, 009 (2014), arXiv:1309.7994 [astro-ph.CO].
[16] T. Kahniashvili, Y. Maravin, A. Natarajan, N. Battaglia, and A. G. Tevzadze, Astrophys. J. **770**, 47 (2013), arXiv:1211.2769 [astro-ph.CO].
[17] M. Shiraishi, H. Tashiro, and K. Ichiki, Phys. Rev. D **89**, 103522 (2014), arXiv:1403.2608.
[18] H. Tashiro and N. Sugiyama, Mon. Not. R. Astron. Soc. **372**, 1060 (2006), astro-ph/0607169.
[19] D. R. G. Schleicher, R. Banerjee, and R. S. Klessen, Astrophys. J. **692**, 236 (2009), arXiv:0808.1461.
[20] Planck Collaboration, P. A. R. Ade, N. Aghanim, M. Arnaud, F. Arroja, M. Ashdown, J. Aumont, C. Baccigalupi, M. Ballardini, A. J. Banday, and et al., ArXiv e-prints (2015), arXiv:1502.01594.
[21] T. Venumadhav, A. Oklopcic, V. Gluscevic, A. Mishra, and C. M. Hirata, ArXiv e-prints (2014), arXiv:1410.2250.
[22] P. Madau, A. Meiksin, and M. J. Rees, Astrophys. J. **475**, 429 (1997), astro-ph/9608010.
[23] A. Loeb and M. Zaldarriaga, Physical Review Letters **92**, 211301 (2004), astro-ph/0312134.
[24] L. J. Greenhill and G. Bernardi, ArXiv e-prints (2012), arXiv:1201.1700 [astro-ph.CO].
[25] J. D. Bowman, M. F. Morales, J. N. Hewitt, and MWA Collaboration, in *American Astronomical Society Meeting Abstracts #218* (2011) p. 132.06.
[26] A. R. Parsons, A. Liu, J. E. Aguirre, Z. S. Ali, R. F. Bradley, C. L. Carilli, D. R. DeBoer, M. R. Dexter, N. E. Gugliucci, D. C. Jacobs, P. Klima, D. H. E. MacMahon, J. R. Manley, D. F. Moore, J. C. Pober, I. I. Stefan, and W. P. Walbrugh, Astrophys. J. **788**, 106 (2014), arXiv:1304.4991.
[27] C. L. Carilli, ArXiv e-prints (2008), arXiv:0802.1727.
[28] K. Vanderlinde and Chime Collaboration, in *Exascale Radio Astronomy* (2014) p. 10102.
[29] D. R. DeBoer and HERA, in *American Astronomical Society Meeting Abstracts*, American Astronomical Society Meeting Abstracts, Vol. 225 (2015) p. 328.03.
[30] H. Yan and A. Lazarian, Astrophys. J. **677**, 1401 (2008), arXiv:0711.0926.
[31] H. Yan and A. Lazarian, J. Quant. Spec. Rad. Trans. **113**, 1409 (2012), arXiv:1203.5571 [astro-ph.GA].
[32] M. Tegmark and M. Zaldarriaga, Phys. Rev. D **79**, 083530 (2009), arXiv:0805.4414.
[33] T. Okamoto and W. Hu, Phys. Rev. D **67**, 083002 (2003), astro-ph/0301031.
[34] Y. Mao, M. Tegmark, M. McQuinn, M. Zaldarriaga, and O. Zahn, Phys. Rev. D **78**, 023529 (2008), arXiv:0802.1710.
[35] A. Mesinger, S. Furlanetto, and R. Cen, Mon. Not. R. Astron. Soc. **411**, 955 (2011), arXiv:1003.3878.
[36] K. M. Górski, E. Hivon, A. J. Banday, B. D. Wandelt, F. K. Hansen, M. Reinecke, and M. Bartelmann, Astrophys. J. **622**, 759 (2005), astro-ph/0409513.